

Workflow and Methods of High-Content Time-Lapse Analysis for Quantifying Intracellular Calcium Signals

Fuhai Li · Xiaobo Zhou · Jinmin Zhu · Weiming Xia ·
Jinwen Ma · Stephen T. C. Wong

Published online: 28 May 2008
© Humana Press 2008

Abstract Calcium ions (Ca^{2+}) play a fundamental role in a variety of physiological functions in many cell types by acting as a secondary messenger. Variation of intracellular Ca^{2+} concentration ($[\text{Ca}^{2+}]_i$) is often observed when the cell is stimulated. However, it is a challenging task to automatically quantify intracellular $[\text{Ca}^{2+}]_i$ in a population of cells. In this study, we present a workflow including specific algorithms for the automated intracellular calcium signal analysis using high-content, time-lapse cellular images. The experimental validations indicate the effectiveness of the proposed workflow and algorithms. We applied the workflow to analyze the intracellular calcium signals induced by different concentrations of H_2O_2 in the

cell lines transfected by presenilin-1 (PS-1) that is known to be closely related to the familial Alzheimer's disease (FAD). The analysis results imply an important role of mutant PS-1, but not normal human PS-1 and mutant human amyloid precursor protein (APP), in enhancing intracellular calcium signaling induced by H_2O_2 .

Keywords High content image analysis · Oxidative stress · Calcium oscillation · Familial Alzheimer's disease · Mutant presenilin 1

Introduction

Alzheimer disease (AD) is a progressive neurodegenerative disease that causes dementia. The neuropathological hallmarks of AD include a progressive loss of neurons, synaptic degeneration, and a deposition of amyloid plaques and neurofibrillary tangles in specific brain regions (LaFerla 2002; Hardy and Selkoe 2002). Ca^{2+} play an important role in many neural processes in AD, e.g. the proper calcium signaling is known to be crucial for synaptogenesis and dendritic spine plasticity (LaFerla 2002; Smith et al. 2005). A number of studies have reported different mechanisms by which intracellular calcium levels are affected (Smith et al. 2005; Zhou et al. 1996; Tu et al. 2006) in AD. However, the dysregulation of calcium homeostasis during AD development is not yet clearly understood. Therefore, study of intracellular calcium signal is very important to understand the underlying mechanisms of the calcium signaling processes, and develop therapeutic strategies aiming to correct calcium dysregulation that may benefit to slow down the progression of AD (LaFerla 2002).

High-content screening (HCS) has recently become an important and widely used technology in disease diagnosis,

F. Li, X. Zhou and J. Zhu contributed equally to this work.

F. Li · J. Ma
Department of Information Science, School of Mathematical Sciences, and LMAM, Peking University,
Beijing 100871, China

F. Li · X. Zhou · S. T. C. Wong
The Center for Biomedical Informatics, The Methodist Hospital
Research Institute, Weill Cornell Medical College,
Houston, TX 77030, USA

X. Zhou · S. T. C. Wong (✉)
Research Division, Department of Radiology, The Methodist
Hospital, Weill Cornell Medical College,
Houston, TX 77030, USA
e-mail: stwong@tmhs.org

J. Zhu
Functional and Molecular Imaging Center, Brigham and Women's
Hospital, Harvard Medical School,
Boston, MA 02115, USA

W. Xia
Department of Neurology, Center for Neurologic Diseases,
Brigham and Women's Hospital, Harvard Medical School,
Boston, MA 02115, USA

drug target validation, and compound screening (Zhou and Wong 2006). Using the HCS technology, the intracellular calcium signals can be represented by the fluorescence intensity of the cells caused by the binding of Ca^{2+} ions with fluo-4 or other Ca^{2+} indicator dyes (Kaestner et al. 2006; Jedrusik et al. 2007). Therefore, HCS enables the quantitative analysis of the intracellular calcium signals at the single cell level using time-lapse cellular images. Since it is not feasible to manually analyze and quantify a large number of time-lapse images at the single cell level, a fully automated and reliable computerized system is therefore needed. However, the existing HCS image analysis tools are inadequate to process the calcium signal images, and this motivated us to propose a new workflow for calcium signal image analysis using time-lapse images. To the best of our knowledge, this is among the first efforts to develop a fully automated HCS workflow with properly designed algorithms for the quantification of intracellular calcium signals at the single cell level.

The integration and implementation of these algorithms in the workflow requires a significant amount of effort and new insights into applying these algorithms. Despite the fact that a number of techniques for the sub-components of the workflow have been previously reported, no single method can be used for a different application without alteration. The main challenges in cell segmentation arise due to cell touching, different cell shapes, variations of cell size, and low intensity contrast (Adiga et al. 2006; Nattkemper 2004). In two separate papers by Lin et al. (2003, 2005), the intensity gradient and shape information are combined to separate the clustered nuclei. However, when the shape of cells cannot be well outlined, for example, the method will fail in segmenting the cells with low intensity contrast. In the case of active contour methods (Osher and Sethian 1988; Malladi et al. 1995; Sethian 1999; Xiong et al. 2005; Xu and Prince 1998), the segmentation results strongly depend on the initialization of the cell boundaries. Some rigid registration methods have been implemented in the National Library of Medicine Insight Segmentation and Registration Toolkit (ITK) (<http://www.itk.org/>) for image displacement correction. However, all of these methods make use of the intensity correlation between the fixed and moving images. Therefore, they fail due to the variation of intracellular calcium signals over time.

In this study, we present a novel computational system for automated calcium signal analysis at the single cell level using time-lapse images. Figure 1 provides a flowchart of the proposed workflow that consists of three major modules: cell segmentation, image displacement correction, and calcium signal analysis, with the introduction of some novel algorithms. The rest of this paper is organized as follows: in the “Materials and Methods” section, we present the detailed information of the cellular images, and the

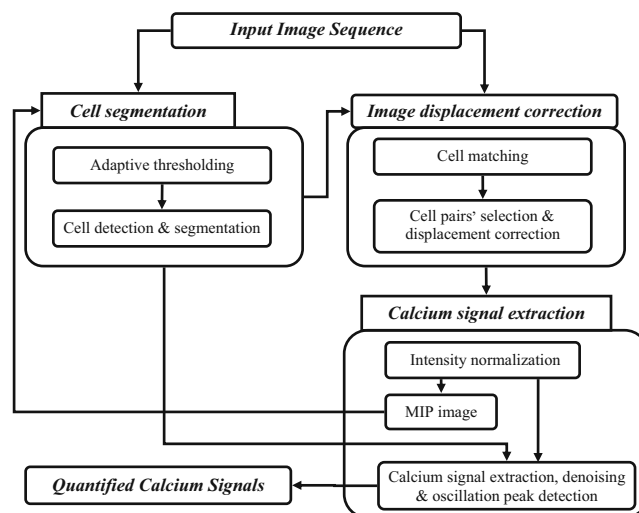


Fig. 1 Flowchart of the proposed intracellular calcium signal analysis system

implementation details of the workflow; the experimental validation, application on the real data, and discussion are provided in the “Results and Discussion” section; and the conclusion remark is given in “Conclusions” section.

Materials and Methods

Materials

In this study, we used four cell lines: Chinese Hamster Ovary (CHO), CHO stably transfected with human APP (7W), CHO stably transfected with human mutant presenilin-1, M146L (ML60), and CHO stably transfected with Human wild-type (PS106). These four cell lines were grown in the conditions as published previously by Xia et al. (1997). In brief, after the cells were loaded and attached to 96 well plates, the cells were treated with Fluo-4 plus F127 (4M/5M, both from Molecular Probes, Invitrogen) in Dulbecco's Modified Eagle's Medium (DMEM) without Ca^{2+} and Fetal Bovine Serum with/without H_2O_2 , incubated at 37 °C for 30 minutes, and then 25 for another 30 minutes. The plates were then moved to the IN Cell Analyzer 1000 (GE Healthcare Life Sciences) for imaging. We collected images every one minute for a total of 120 minutes for each well. Hoechst staining (Molecular Probes, Invitrogen) of cell nuclei was also employed in the incubation of the cells to count the total cell number. Figure 2 provides one example image generated in this study.

Cell Segmentation

To extract the calcium signals inside cells, we needed to segment cells accurately. The initial cell segmentation results were also needed for the subsequent displacement correction

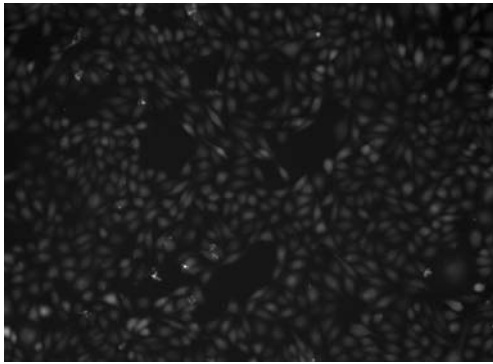


Fig. 2 Representative cellular images generated in this study

algorithm. In the proposed segmentation method, we first separated cell pixels from the background using an adaptive thresholding method (Sahoo et al. 1988; Sezgin and Sankur 2004; Wahlby et al. 2002; Lindblad et al. 2004; Otsu 1978). Although cells are separated from the background using the adaptive thresholding method, the cell clusters cannot be separated. Cell detection is very important in order to separate the cell clusters by identifying ‘seeds’ or initial contours for the subsequent segmentation methods, e.g. marker controlled watershed, Voronoi, level set, and sneak algorithms. We propose a cell detection method using the Gaussian filtering (Lindeberg 1998) and gradient vector field (GVF). Finally, the clustered cells are segmented using the cell detection results and marker controlled watershed method (Adiga et al. 2006; Lin et al. 2003; Beucher 1992; Vincent and Soille 1991).

Adaptive Thresholding Global threshold, e.g. Otsu thresholding, cannot generate good binary results because the intensity of the cells (calcium signals) is uneven. Herein, an adaptive thresholding algorithm is implemented based on a background correction method (Wahlby et al. 2002; Lindblad et al. 2004). The adaptive thresholding method can be written as:

$$C(x, y) = q(I(x, y) - B(x, y) - c * \sigma_B); \quad (1)$$

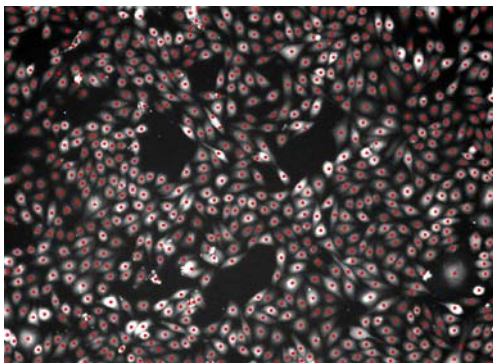


Fig. 3 Representative cell detection result using the proposed cell detection method

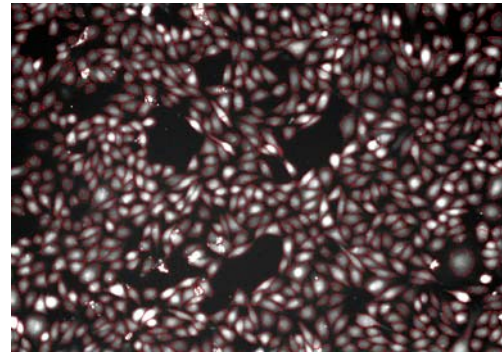


Fig. 4 Representative cell segmentation result using the detection results

where $I(x, y)$ is the cellular image; $B(x, y)$ is the estimated background image; c is a control parameter; more pixels are classified into background with a larger value of c , and more pixels are classified into object with smaller value of c . We set $c=1.5$ experimentally. σ_B is the standard deviation of $B(x, y)$. $q(z)$ is an indicator function: if $z \geq 0$, $q(z)=1$, else $q(z)=0$. If $C(x, y)=1$, pixel (x, y) is classified as a part of the object, otherwise, the pixel (x, y) is classified as a part of the background. In the binary image, the noisy fragments are removed based on their size, and the small holes are filled by removing them as the noisy fragments in the inverse image.

Cell Detection and Segmentation To detect the cell centers, we first suppress the noisy intensity maxima using Gaussian filtering with appropriate scale σ . The value of σ can be chosen based on test images. In the filtered image, the noises are suppressed and the local maxima correspond to the cell centers. However, some noises still exist. To further eliminate the noisy local maxima, we detect the true cell centers in the gradient vector field (GVF) by counting the number of particles converging towards them, which is described as follows. It is a well-known fact that in an electric field, the electric field lines point to the positive electrodes, and the free negative electrons move along the electric field lines and stop at these electrodes. In GVF, the gradient-vector lines also point to the local maxima. Analogous to the electron moving inside the electron field, we put one particle on each detected cell pixel and pushed it along the gradient vector lines. Consequently, these particles stopped at these local maxima. The movement of the particle is described in the pseudo code as shown in the next page. Since no or very few particles stop at non-maxima and noisy local maxima, the true cell centers can be identified by choosing the points that have many particles. Finally, cell clusters are separated using the marker-controlled watershed algorithm. The representative detection and segmentation results are provided in Figs. 3 and 4, respectively.

Particle moving in gradient vector field (GVF) algorithm

```

Mcel; /*Detected cell pixel matrix in which the value of background pixel is 0 and cell
pixel is 1*/
Mgvf; /*Gradient vector field matrix which consists of the gradient vectors of each
pixel*/
Mpar ← zeros(m,n);
/*Particle distribution matrix whose elements are the number of particles that stop at each
pixel. We initialize its elements as 0*/
while(ExistNonZero(Mcel))
    (x0, y0) = find(Mcel == 1); /*find one detected cell pixel*/
    (x1, y1) = (0,0); /*(x1, y1) is used to record the stop pixel of the particle which is
put on the (x0, y0)*/
    while((x1, y1) != (x0, y0))
        (x1, y1) = move((x0, y0), Mgvf(x0, y0));
        /*move the particle from (x0, y0) along the direction of Mgvf(x0, y0) to
pixel (x1, y1). If pixel (x0, y0) is a local maximum, the gradient vector
Mgvf(x0, y0) will point to itself, and (x1, y1) == (x0, y0) which means the
particle stop at this point*/
    end
    Mpar(x1, y1) = Mpar(x1, y1) + 1;
    /*the number of particles stop at pixel (x1, y1) increases one*/
end

```

Image Displacement Correction

In sequential image processing, the image displacement correction is necessary due to the displacement of the positions of the microscope in different time points (Gustavsson et al. 2003). Since the cells are stationary in the images, the displacement between two consecutive frames is the same as the displacement of cells inside them. In other words, we can correct the displacement of two consecutive frames using the average of the displacements of *some of the selected cells* inside them. This method using a few instead of all of the cells in the frame is necessary because using all of the cells would require much more computation. Moreover, the cells with low intensity contrast cannot be used because their displacement information is unreliable because of their inaccurate segmentation.

Cell Matching To compute the displacement of cells in two consecutive frames, we need to do the cell matching first. In other words, given one cell in the current frame, we need to find the corresponding cell in the successive frame. In this study, we used an overlap area based cell matching method (Chen et al. 2006). For easy understanding of this method, the detailed definition of the dissimilarity measurement can be written as:

$$d_{i,j}(t) = \begin{cases} 1 - \frac{A_i(t) \cap A_j(t+1)}{A_i(t) \cup A_j(t+1)}, & A_i(t) \cap A_j(t+1) \neq 0; \\ 1 + \frac{\text{dis}\{O_i(t), O_j(t+1)\}}{R_i(t) + R_j(t+1)}, & A_i(t) \cap A_j(t+1) = 0. \end{cases} \quad (2)$$

where $d_{i,j}(t)$ denotes the similarity measure between the i -th cell in frame t , $C_i(t)$, and the j -th cell in frame $t+1$, $C_j(t+1)$; $A_i(t)$, $A_j(t+1)$, $O_i(t)$, $O_j(t+1)$ and $R_i(t)$, $R_j(t+1)$ are the area, centroids, and radii of the cells $C_i(t)$ and $C_j(t+1)$; $\text{dis}\{O_i(t)$,

$O_j(t+1)$ means the distance between the centroids $O_i(t)$ and $O_j(t+1)$. Then, the cell matching is done by choosing their nearest neighbor.

Cell Pairs' Selection and Displacement Correction Since it is reasonable that cells with higher intensity contrast have higher possibility to be well segmented, we select cells used for the displacement correction with the following two steps: first, the minimum average intensity of one cell and its matching cell $C_j(t+1)$, denoted by $Avg_{i,j}(t)$, is defined as:

$$Avg_{i,j}(t) = \min\{Avg_i(t), Avg_j(t+1)\} \quad (3)$$

where $Avg_i(t)$ and $Avg_j(t+1)$ are the average intensity of cell and $C_j(t+1)$ respectively; secondly, the cells are selected according their minimum average intensity in the descending order. Then, the displacement of two consecutive frames is corrected based on the average of the displacements of the selected cells in the two frames. In this study, 100 cell pairs inside two consecutive frames are selected for the displacement correction.

Calcium Signal Analysis

The $[Ca^{2+}]_i$ inside cells are represented by the average of fluorescence intensity of the cells as:

$$[Ca^{2+}]_i = K_d \frac{F - F_{\min}}{F_{\max} - F_{\min}} \quad (4)$$

where K_d is the ion dissociation constant ($K_d=345nM$), F_{\min} is the fluorescence intensity in the absence of calcium, F_{\max} is the fluorescence intensity in the saturation of calcium, and F is the average fluorescence intensity of the cells (Woodruff et al. 2002).

Intensity Normalization To reduce the influence of the variation of background, an intensity normalization method is implemented. First, the background of each frame is estimated using the cubic B-spline (Lindblad et al. 2004; Otsu 1978). Then, we use the estimated background to perform intensity normalization as:

$$I'(x, y; t) = \frac{B(x, y; 1)}{B(x, y; t)} I(x, y; t), \quad t = 2, 3, \dots, N. \quad (5)$$

where $I(x, y; t)$ is the t -th intensity normalized image; $B(x, y; 1)$ and $B(x, y; t)$ are the estimated background of the first and t -th frames, $I(x, y; t)$ is the t -th aligned image. After intensity normalization according to Eq. (5), all frames have roughly the same gray level background as that of the first frame, so the variation of the background is effectively reduced.

Calcium Signal Extraction and Denoising After displacement correction and intensity normalization, the maximum intensity projection (MIP) image, denoted by $I_{\text{mip}}(x, y)$, is generated as follows:

$$I_{\text{mip}}(x, y) = \max_{t \in [1, N]} \{I'(x, y; t)\} \quad (6)$$

where $I'(x, y; t)$ is the t -th intensity normalized image, and N is the number of frames. In the MIP image, cells have their highest intensity over all frames, as seen in Fig. 5. Figure 5a shows part of the MIP image; Fig. 5b and c are parts of two single frames. Hence, we can segment all of the cells accurately in the MIP image using the proposed segmentation method. Then, the 3D cell boundaries (x, y, t) can easily be constructed by placing the boundaries of cells on each aligned frame. Finally, the calcium signal inside each cell is extracted by averaging the fluorescence intensity of cells and translated according to equation (5). In the extracted calcium signals, noisy signals will most likely be induced by the bias of segmentation, displacement correction, and intensity normalization. To suppress these noisy signals, the undecimated discrete wavelet transform (UDWT) (Coombes et al. 2005) is employed. Figure 6 provides an example of extracted calcium signals.

Oscillation Peak Detection In this study, two patterns are observed in the extracted calcium signals: some calcium signals remain constant, whereas others have oscillation peaks. To detect the oscillation peaks of the second pattern, a peak detection method is implemented. The idea of this method arises from the fact that a local minimum appears immediately following a local maximum in the first-order backward differential signals, as seen in Fig. 7b. The peak detection method consists of three steps: (1) the first-order backward difference of the calcium signal is calculated; (2) the local maxima and minima whose absolute values are larger than a given threshold, e.g. the standard deviation of the signal, are detected; and (3) the points, around which the detected local maximum and minimum appear in sequence, are identified as the oscillation points.

Results and Discussion

Validation of Segmentation

To evaluate the accuracy of the proposed segmentation method, we randomly selected 16 cellular images from four image sequences: three single frames and the MIP image in each sequence. Four kinds of errors may occur in cell segmentation: over-segmentation, under-segmentation, false negative (missed cell), and false positive (noise).



(a)



(b)



(c)

Fig. 5 Comparison between the MIP image and single frames. (a) MIP image. (b), (c) are two single frames

Two biologists validated these segmented images by manually counting the numbers of cells and the four kinds of errors based on their experience. Table 1 provides the average of the validations provided by the two biologists. On an average, 96.6% of the cells were correctly segmented; 1.2% of the cells were over-segmented; 0.7% of cells were under-segmented; the false negative rate was 1.8% and the false positive rate was 0.4%. The experimental results indicate that the proposed segmentation method works effectively for this study. Analyzing the four kinds of

errors, we concluded that the over-segmentation problem often occurs in the elongated cells in which some redundant maxima are not suppressed successfully. The missed cells have very low intensity contrast, and it is difficult to segment them even manually. The few false positives were caused by the noise speckles. Under-segmentation occurred when a cell with low intensity overlapped with another cell with higher intensity. This happens due to the fact that only one local maximum is generated inside the cell with strong intensity. We intend to address these problems in the future.

Validation of Displacement Correction

To quantitatively validate the displacement correction, the intensity difference between the fixed and moving images is often used. However, it is not suitable for this study due to the variation of calcium signals over time. Herein, we randomly selected the MIP images of 50 sequences. Two biologists validated these MIP images using three scores: clear, blurry, bad. Three MIP images were marked as 'blurry' by both biologists; one MIP image was labeled as 'blurry' by one biologist. The rest of the 46 images were marked 'clear', and no sequence was marked as 'bad'. To further evaluate the displacement correction method, we compared the rigid registration method in ITK with our method. We selected two sequences: one sequence almost has no displacement, and the other has a significant amount of displacement. Figure 8 shows the displacement correction results. As we can see, the rigid registration method in ITK generates bad correction results for both of the sequences, while the proposed method is accurate and reliable for our image data.

Validation of Extracted Calcium Signals

In this study, three patterns of calcium signals were found: stable, 'break out', and oscillating. Figure 6a–f show the representative images of these three patterns respectively. To validate the extracted calcium signals, we randomly selected 100 calcium signals in each of the four image sequences. For convenience, we viewed both the 'break out' and oscillating patterns as one (oscillation) class. Our biologists validated these calcium signals by comparing them with their investigations. If the number and positions of the strong oscillation peaks of the extracted calcium signals were consistent with their investigation results, the signal was labeled 'C' to denote a correctly extracted calcium signal, otherwise the signal was labeled 'W' to denote a wrongly extracted calcium signal. The experimental results demonstrated that all 400 calcium signals were correctly extracted. This result shows that the proposed calcium signal extraction method is reliable. Therefore, the biologists can conveniently investigate the calcium signal inside any cell and analyze them quantitatively.

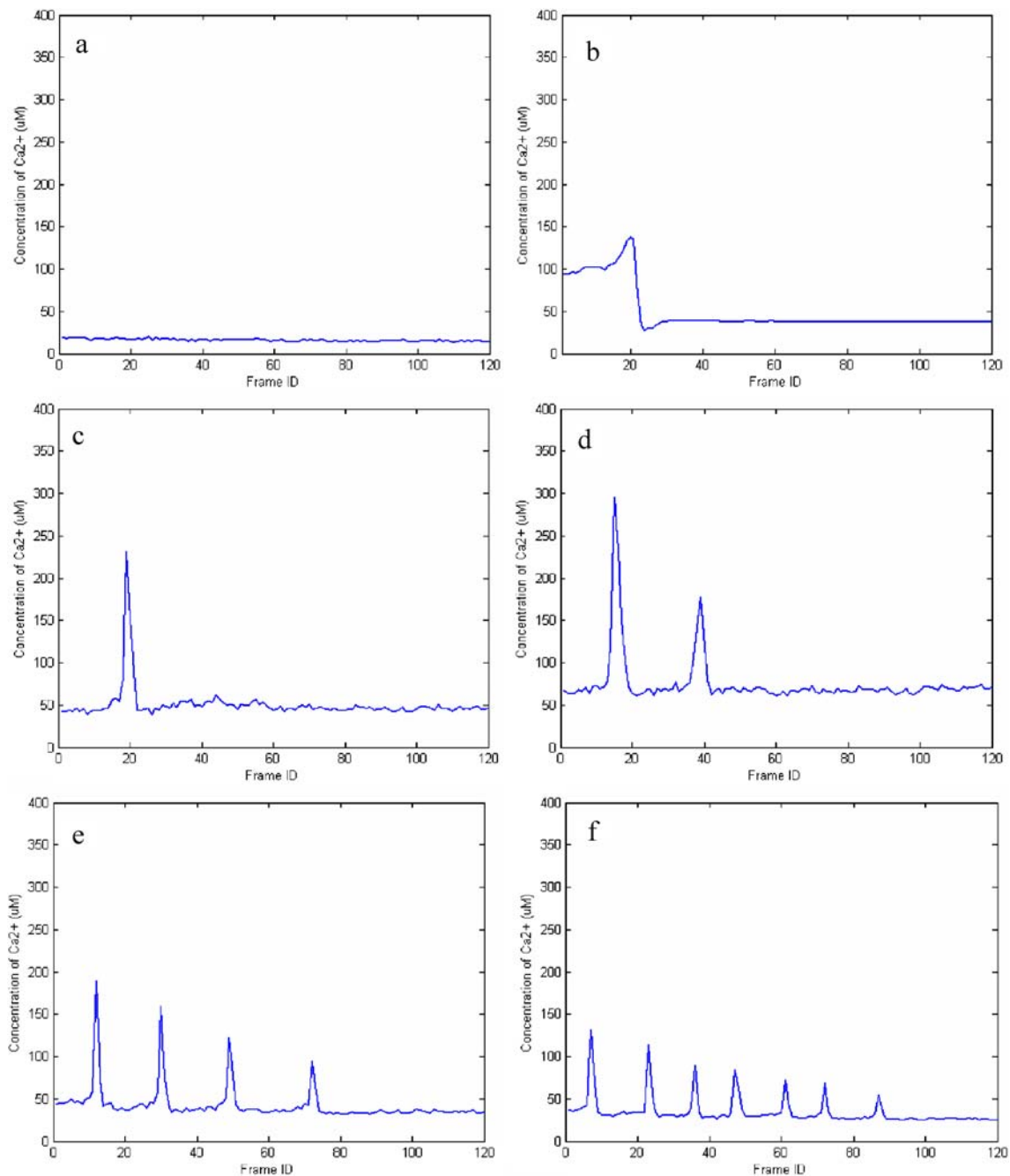


Fig. 6 Representative extracted intracellular calcium signals. **(a)** Representative stable calcium signal. **(b)** Representative ‘break out’ calcium signal that reflects the cell dying at the jump point. **(c), (d), (e), (f)** Representative oscillating calcium signals

Analysis of Calcium Signals Inside Cells Expressing HAD PS-1 Exposed to H_2O_2

FAD has close relationship with the mutation of the PS-1 gene. FAD caused by this mutation leads to the over production of amyloid- β ($A\beta$) and closely associates with dysregulation of calcium homeostasis (Smith et al. 2005; Stutzmann 2005; Xia 2000) and the reactive oxygen species, e.g. H_2O_2 , were found to increase intracellular calcium levels (Fowler et al. 1998). The reactive oxygen

species can be formed by $A\beta$ in cultured neurons, and can be generated in response to mitochondrial dysfunction or microglial activation (Hensley et al. 1994; Blass et al. 1990; Colton and Gilbert 1987). In this study, we propose using a high-content time-lapse cell imaging method to understand the mechanisms between the oxidative stress and calcium signals inside cells transfected by PS-1 mutations. We designed an experiment as follows: Four aforementioned cell lines were selected and treated with six different concentrations of H_2O_2 : 0.001, 0.01, 0.1, 1, 10, and

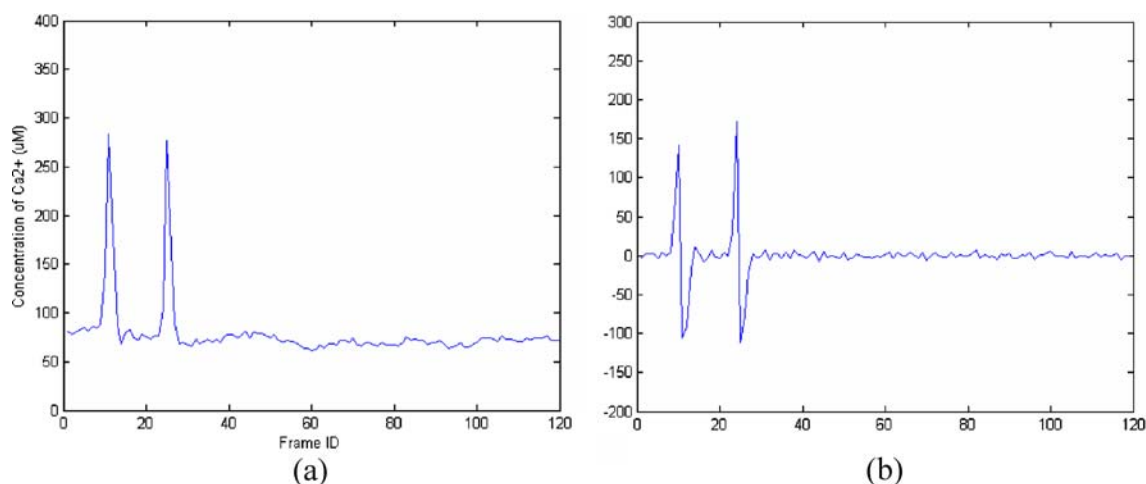


Fig. 7 Illustration of the peak detection. (a) Extracted calcium signal. (b) First order differential signal

100 µM. Their cellular images were acquired by the GE IN Cell Analyzer 1000. Using the proposed system, the calcium reaction signals inside the cells were extracted and analyzed.

As previously mentioned, three patterns of calcium signals were found. The ‘break out’ pattern was investigable in all of four cell lines treated with 10 and 100 µM H₂O₂. In the ‘break out’ pattern, the [Ca²⁺]_i jumps rapidly and drops down deeply just before the cells are killed due to the deleterious effect of H₂O₂. Averaged, the intracellular calcium concentrations of cells treated with 10 and 100 H₂O₂ are higher than that of cells treated with the lower concentrations of H₂O₂. The oscillating pattern is mainly

investigated in cell sequences treated with 0.001, 0.01, 0.1 and 1 µM H₂O₂. Figure 9 provides the percentage of oscillating cells of four cell lines treated with 0.001, 0.01, 0.1 and 1 µM H₂O₂. As we can see, there are much more oscillation response cells in the ML60 cell line than the other three cell lines. To test for differences in cell oscillations caused by the cell line, the H₂O₂ level, and due to the interaction between the two, we first performed the two-way ANOVA analysis (Cobb 1998; Dukes and Sullivan 2007; Hsu 1996). As seen in Table 2, the effects of the cell line are significant while the effects of H₂O₂ level and interaction between them are not significant. Further, to find out which cell line effects differ from each other, the

Table 1 Validation of the proposed segmentation method using 16 selected images

Images	No. of cells (manual counted)	No. of cells (correctly segmented)	No. of cells (over-segmented)	No. of cells (under-segmented)	No. of cells (missed)	No. of cells (noise)
1	881	842 (95.6%)	4 (0.5%)	7 (0.8%)	28 (3.2%)	0 (0.0%)
2	878	837 (95.3%)	13 (1.5%)	11 (1.3%)	17 (1.9%)	0 (0.0%)
3	832	798 (95.9%)	8 (1.0%)	9 (1.1%)	17 (2.0%)	0 (0.0%)
4	864	844 (97.7%)	2 (0.2%)	4 (0.5%)	14 (1.6%)	0 (0.0%)
5	636	610 (95.9%)	18 (2.8%)	2 (0.3%)	6 (1.0%)	4 (0.6%)
6	632	605 (95.7%)	21 (3.3%)	2 (0.3%)	4 (0.6%)	11 (1.7%)
7	629	597 (94.9%)	26 (4.1%)	1 (0.2%)	5 (0.8%)	12 (1.9%)
8	612	593 (96.9%)	10 (1.6%)	1 (0.2%)	8 (1.3%)	14 (2.28%)
9	874	850 (97.3%)	16 (1.8%)	2 (0.2%)	6 (0.8%)	4 (0.5%)
10	919	893 (97.2%)	11 (1.2%)	3 (0.3%)	12 (1.3%)	2 (0.2%)
11	923	904 (97.9%)	10 (1.1%)	4 (0.4%)	5 (0.5%)	5 (0.5%)
12	906	877 (96.8%)	5 (0.6%)	1 (0.1%)	23 (2.5%)	1 (0.1%)
13	972	942 (96.9%)	3 (0.3%)	4 (0.4%)	23 (2.4%)	2 (0.2%)
14	998	969 (97.1%)	5 (0.5%)	4 (0.4%)	20 (2.0%)	1 (0.1%)
15	979	947 (96.7%)	3 (0.3%)	7 (0.7%)	22 (2.2%)	0 (0.0%)
16	995	959 (96.4%)	2 (0.2%)	1 (0.1%)	33 (3.3%)	0 (0.0%)
Avg.	846	817 (96.6%)	10 (1.2%)	4 (0.7%)	15 (1.8%)	4 (0.4%)

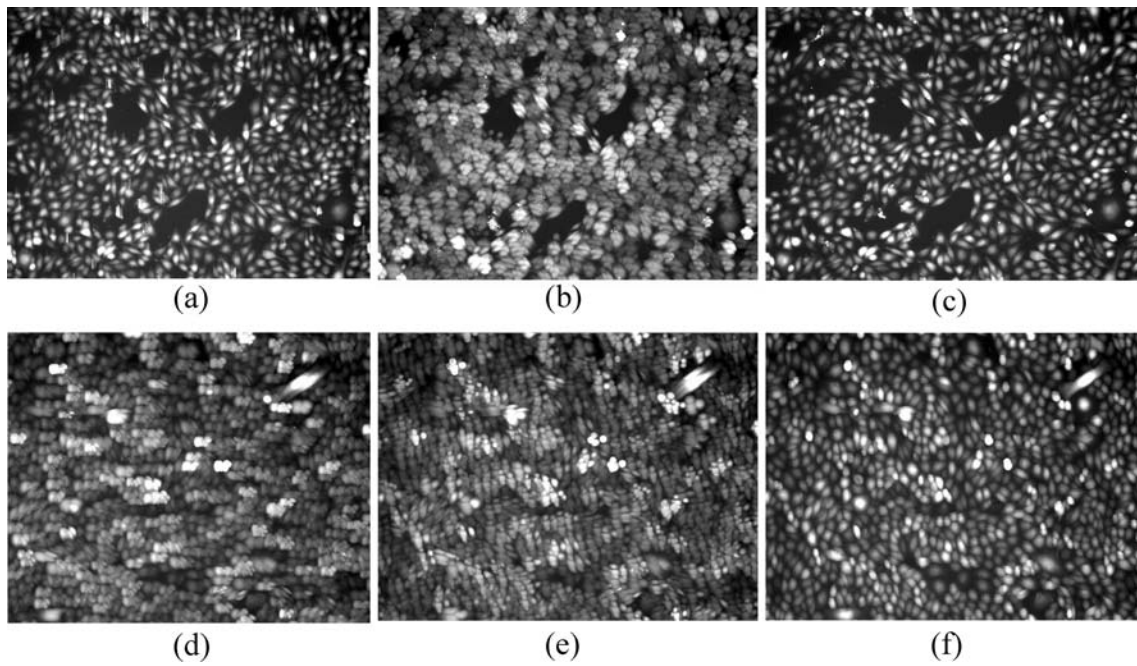


Fig. 8 Comparisons between the rigid registration method in ITK and the proposed method. (a), (d) MIP images of two selected sequences without registration. (b), (e) MIP images after using rigid registration method in ITK. (c), (f) MIP images after using the proposed displacement correction method

Fig. 9 Diagram of percentages of oscillating cells of four cell lines in four different concentrations of H₂O₂

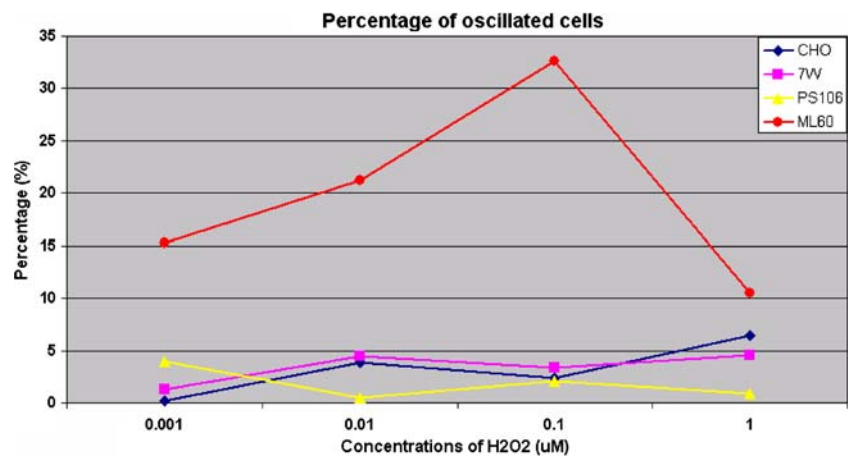


Table 2 Results of two-way ANOVA ($\alpha=0.05$)

Source of the variability	Sum of squares	Degrees of freedom	Mean squares	F-critical	P-value
Cell line	1804.98	3	601.661	11.02	0.004
H ₂ O ₂ level	139.81	3	46.604	0.85	0.4849
Interaction	468.27	9	52.03	0.95	0.5096
Error	873.46	16	54.591	–	–
Total	3286.53	31	–	–	–

Table 3 Results of Tukey–Kramer multiple comparison ($\alpha=0.05$)

Group pairs	Estimated mean difference	Confidence interval	Is difference significant?
(CHO, ML60)	-16.69	[-26.62, -6.76]	Yes
(CHO, PS106)	1.85	[-8.08, 11.78]	No
(CHO, 7W)	-0.19	[-10.12, 9.74]	No
(ML60, PS106)	18.55	[8.62, 28.48]	Yes
(ML60, 7W)	16.50	[6.57, 26.43]	Yes
(PS106, 7W)	-2.05	[-11.98, 7.88]	No

Tukey–Kramer multiple comparison (Hsu 1996) test was employed, as seen in Table 3. We can see that there are significant differences between the ML60 and the three other cell lines, while there is no significant differences between the CHO, 7W, and PS106. Through the experimental results, we conclude that the oscillating response cells in the mutant PS-1 cell line (ML60) are more easily detectable in all four concentrations of H_2O_2 than that of the three other cell lines. The evidence obtained implies an important role of mutant PS-1, but not normal human PS-1 and mutant human APP, in enhancing intracellular calcium signaling induced by H_2O_2 .

Discussion

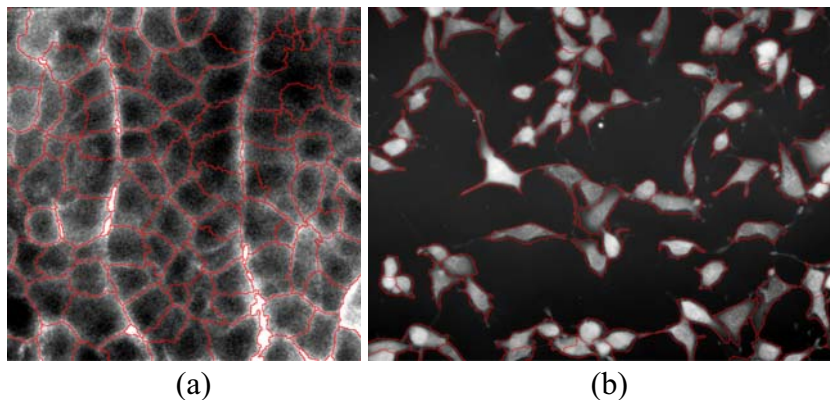
In this study, we proposed an automatic workflow for quantitative analysis of intracellular calcium signals with well designed algorithms. The practical application of analyzing the intracellular calcium signals of four cell lines indicates the effectiveness of the proposed workflow. This workflow was designed mainly for cultured cells. The quality of the cellular images *in vivo* is often worse than the cultured cellular images. Our algorithm was tested on one *in vivo* cellular image and, as shown in Fig. 10a, the segmentation result was acceptable. Therefore, the proposed workflow can be used for some *in vivo* cellular images. We also tested the cultured neuron cell images and

determined that, if the neurites are not very complex, the segmentation result is acceptable, as seen in Fig. 10b. Therefore, the proposed workflow can process some cultured neuron cells as well. Since the structure of the neuron images *in vivo* is totally different with the cells we used, the proposed workflow is not currently suitable for them. The input of the proposed system is the time-lapse cellular images whose intensity characterizes the calcium signals inside cells. The output of the system is the intensity of single cells over time, which is then mapped into the true calcium signals. Therefore, the calcium indicators, for example, fluo-3, fluo-4, that can be quantitatively acquired by the microscope can be processed using the proposed workflow.

Conclusions

In this study, we have proposed a computerized system to automate high-content, cellular image sequence analysis for the quantification of calcium signals at the single cell level. The proposed cell detection method detects the cells effectively. The displacement correction method can generate reliable results using the cell matching method. The proposed intensity normalization method ensures all the frames have a similar gray level of background. To avoid the low intensity contrast problem, we delineate the boundaries of cells in the MIP image. Finally, the calcium

Fig. 10 Segmentation results of the *in vivo* cellular image and cultured neuron cell image. (a) Segmentation result of *in vivo* cellular image. (b) Segmentation result of the cultured neuron cell image



signals inside cells are quantified accurately, and the oscillation points are detected using the proposed peak detection method. The validation results show that the proposed system is reliable and effective. Using the proposed computerized system, the biologists can conveniently analyze the quantified calcium signals of a population of cells at the single cell level.

Information Sharing Statement

The software is developed in Matlab (version 7.0.1) on Windows XP platform. The sample image sequences and the software are available upon request.

Acknowledgment The authors would like to thank Jian Chen for technique help. This work is supported by NIH R01 LM008696 grant and the Center for Bioinformatics Program grant of Harvard Center of Neurodegeneration & Repair, Harvard Medical School, Boston, USA to STC Wong. Jinmin Zhu is supported by NIH 5K12MH069281-04.

References

- Adiga, U., et al. (2006). High-throughput analysis of multispectral images of breast cancer tissue. *IEEE Transactions on Image Processing*, *15*, 1057–1149.
- Beucher, S. (1992). The watershed transformation applied to image segmentation. *Scanning Microscopy International*, *6*, 299–314.
- Blass, J., et al. (1990). Induction of Alzheimer antigens by an uncoupler of oxidative phosphorylation. *Archives of neurology*, *47*(8), 864–869.
- Chen, X., Zhou, X., & Wong, S. (2006). Automated segmentation, classification, and tracking of cancer cell nuclei in time-lapse microscopy. *IEEE Transactions on Biomedical Engineering*, *53* (4), 762–766.
- Cobb, G. W. (1998). *Introduction to design and analysis of experiments*. New York: Springer Verlag.
- Colton, C. A., & Gilbert, D. L. (1987). Production of superoxide anions by a CNS macrophage, the microglia. *FEBS Letter*, *223*(2), 284–288.
- Coombs, K. R., et al. (2005). Improved peak detection and quantification of mass spectrometry data acquired from surface-enhanced laser desorption and ionization by denoising spectra with the undecimated discrete wavelet transform. *Proteomics*, *5*, 4107–4117.
- Dukes, K. A., & Sullivan, L. M. (2007). *A review of basic biostatistics*. Cambridge, MA: Cell Press.
- Fowler, C. J., Ando, Y., & Tiger, G. (1998). Comparison of the effects of hydrogen peroxide, 4-hydroxy-2-nonenal and β -amyloid (25–35) upon calcium signalling. *Neurochemistry International*, *33* (2), 161–172.
- Gustavsson, T., et al. (2003). Time-lapse microscopy and image processing for stem cell research: modeling cell migration. *Proceedings of SPIE*, *5032*, 1–15.
- Hardy, J., & Selkoe, D. J. (2002). The amyloid hypothesis of Alzheimer's disease: progress and problems on the road to therapeutics. *Science*, *297*(5580), 353–356.
- Hensley, K., et al. (1994). A model for beta-amyloid aggregation and neurotoxicity based on free radical generation by the peptide: relevance to Alzheimer disease. *Proceedings of the National Academy of Sciences of the United States of America*, *91*(8), 3270–3274.
- Hsu, J. C. (1996). *Multiple Comparisons Theory and Methods*. London: Chapman & Hall.
- Jedrusik, A., et al. (2007). Mouse oocytes fertilised by ICSI during in vitro maturation retain the ability to be activated after refertilisation in metaphase II and can generate Ca²⁺ oscillations. *BMC Developmental Biology*, *7*, 72.
- Kaestner, L., et al. (2006). Calcium imaging of individual erythrocytes: problems and approaches. *Cell Calcium*, *39*, 13–19.
- LaFerla, F. M. (2002). Calcium dyshomeostasis and intracellular signalling in Alzheimer's disease. *Nature reviews. Neuroscience*, *3*(11), 862–872.
- Lin, G., et al. (2003). A hybrid 3-D watershed algorithm incorporating gradient cues and object models for automatic segmentation of nuclei in confocal image stacks. *Cytometry A*, *56*, 23–36.
- Lin, G., et al. (2005). Hierarchical, model-based merging of multiple fragments for improved three-dimensional segmentation of nuclei. *Cytometry A*, *63*, 20–33.
- Lindblad, J., et al. (2004). Image analysis for automatic segmentation of cytoplasm and classification of Rac1 activation. *Cytometry A*, *57*(1), 22–33.
- Lindeberg, T. (1998). Feature detection with automatic scale selection. *Journal of Computer Vision*, *30*, 79–116.
- Malladi, R., Sethian, J., & Vemuri, B. (1995). Shape modeling with front propagation—a level set approach. *IEEE Transactions on Pattern Analysis and Machine Intelligence*, *21*(10), 404–415.
- Nattkemper, T. (2004). Automatic segmentation of digital micrographs: a survey. *Medical Informatics*, *11*, 847–851.
- Osher, S., & Sethian, J. A. (1988). Fronts propagating with curvature-dependent speed: algorithms based on Hamilton–Jacobi formulations. *Journal of Computational Physics*, *79*, 12–49.
- Otsu, N. (1978). A threshold selection method from gray level histogram. *IEEE Transactions on System, Man, and Cybernetics*, *8*, 62–66.
- Sahoo, P., et al. (1988). A survey of thresholding techniques. *Computer Vision Graphics Image Processing*, *41*, 233–260.
- Sethian, J. A. (1999). *Level set methods and fast marching methods: evolving interfaces in computational geometry, fluid mechanics, computer vision, and materials science*. New York: : Cambridge University Press.
- Sezgin, M., & Sankur, B. (2004). Survey over image thresholding techniques and quantitative performance evaluation. *Journal of Electronic Imaging*, *13*(1), 146–165.
- Smith, I. F., Green, K. N., & LaFerla, F. M. (2005). Calcium dysregulation in Alzheimer's disease: recent advances gained from genetically modified animals. *Cell Calcium*, *38*(3–4), 427–437.
- Stutzmann, G. E. (2005). Calcium dysregulation, IP3 signaling, and Alzheimer's disease. *The Neuroscientist*, *11*, 110–115.
- Tu, H., et al. (2006). Presenilins form ER Ca²⁺ leak channels, a function disrupted by familial Alzheimer's disease-linked mutations. *Cell*, *126*(5), 981–993.
- Vincent, L., & Soille, P. (1991). Watersheds in digital spaces: an efficient algorithm based on immersion simulations. *IEEE Transactions on Pattern Analysis and Machine Intelligence*, *13*, 583–598.
- Wahlby, C., et al. (2002). Algorithms for cytoplasm segmentation of fluorescence labelled cells. *Analytical Cellular Pathology*, *24*(2–3), 101–111.
- Woodruff, M. L., et al. (2002). Measurement of cytoplasmic calcium concentration in the rods of wild-type and transducin knock-out mice. *Journal of Physiology*, *542*, 843–854.

- Xia, W. (2000). Role of presenilin in gamma-secretase cleavage of amyloid precursor protein. *Experimental Gerontology*, 35(4), 453–460.
- Xia, W., et al. (1997). Enhanced production and oligomerization of the 42-residue amyloid beta-protein by Chinese hamster ovary cells stably expressing mutant presenilins. *Journal of Biological Chemistry*, 272, 7977–7982.
- Xiong, G., et al. (2005). Automated segmentation of Drosophila RNAi fluorescence cellular images using deformable models. *IEEE Transactions on Circuits and Systems*, 53, 2415–2424.
- Xu, C., & Prince, J. L. (1998). Snakes, shapes, and gradient vector flow. *IEEE Transactions on Image Processing*, 7, 359–369.
- Zhou, X., & Wong, S. (2006). High content cellular imaging for drug development. *Signal Processing Magazine, IEEE*, 23, 170–174.
- Zhou, Y., Gopalakrishnan, V., & Richardson, J. (1996). Actions of neurotoxic beta-amyloid on calcium homeostasis and viability of PC12 cells are blocked by antioxidants but not by calcium channel antagonists. *Journal of Neurochemistry*, 67, 1419–1425.